Electronic Supplementary Material (ESI) for CrystEngComm.

Two Co(II) complexes containing pyridylbenzimidazole ligands as chemosensors for sensing of levofloxacin, acetylacetone, and Ni^{2+} with high selectivity and sensitivity

Ming-Yue Wen, Li Ren, Guang-Hua Cui*

College of Chemical Engineering, Hebei Key Laboratory for Environment Photocatalytic and Electrocatalytic Materials, North China University of Science and Technology, No. 21 Bohai Road, Caofeidian new-city, Tangshan, Hebei, 063210, P. R. China

* Corresponding author. Fax: +86–315–8805462, Tel: +86–315–8805460.

*E-mail: tscghua@126.com

Materials and methods

All of the reagents and solvents were commercially purchased directly and did not further purified. Elemental analyses were accomplished by a PerkinElmer 240°C analyzer. The X-ray diffraction (XRD) with graphite monochromatized Cu-Kα radiation (λ = 1.5418 Å) were carried out by Rigaku D/Max-2500PC X-ray diffractometer at 40 kV, 40 mA. The FT-IR spectra (4000–400 cm^{-1}) were recorded on a Bruker VERTEX 80 V FTIR spectrophotometer. In the 25–800 °C range, the thermogravimetric analyses (TGA) were obtained by using a Netzsch STA449 F1 thermal analyzer at a heating rate of 10 °C /min under the air atmosphere protection. The fluorescence experiments of **1** and **2** were measured at room temperature on the Edinburgh FS5 fluorescence spectrophotometer.

Single-Crystal X-ray Diffraction

X-ray diffraction data of **1** and **2** were received at room temperature on a Rigaku XtalLabMini diffractometer by monochromated Mo-Ka radiation (λ = 0.71073 Å) adopting ω-scan mode at 296(2) K and further calculated by the CrysAlisPro program. The structures of **1** and **2** were solved by a SHELXT-2015, and further refined by SHELXL-2018/3 with full-matrix least-squares based on F^2. All of the non-hydrogen atoms were anisotropic. The H atoms of organic ligands are included in the calculated positions and the parent atoms are refined using isotropic thermal parameters riding of the parent atoms. The crystallographic data and structure determination statistics for two coordination compounds can be found in Table S1, and the necessary bond distances and angles are listed in Table S2.

Photoelectrochemical properties

The experiments were carried out in a three-electrode cell. As-prepared sample powder dispersed with ethanol was coated onto a slice of ITO glass with an area of 1.0 × 1.0 cm^2 as a

working electrode. A saturated calomel electrode (SCE) and a 0.5 × 0.5 cm^2 Pt plate were used as the reference and counter electrodes, respectively. The electrolyte was 0.1 M Na_2SO_4 aqueous solution. The light source was 300 W Xe lamp. The MottSchottky curves were also measured in 0.1 M Na_2SO_4 aqueous solution. The AC amplitude was set as 10 mV and the frequency was 1000, 1500, 2000 Hz. Electrochemical impedance spectroscopy (EIS) was recorded with a potentiostat/galvanostat. The frequency range was explored from 10 mHz to 0.1 MHz.

Formulas

$$quenching\ efficiency = (I_0 - I)/I_0 \times 100\% \quad (1)$$

where I_0 and I are the maximum fluorescence intensities before and after the addition of the targeted species.

$$I_0/I - 1 = Aexp(R[M]) + b \quad (2)$$

where A, R and b represent constants and [M] is the concentration.

$$y(t) = B_1 e^{-t/\tau_1} + B_2 e^{-t/\tau_2} \quad (3)$$

where τ_1 and τ_2 represent the components of fluorescence lifetime, B_1 and B_2 are the corresponding amplitudes and t is the instantaneous time.

$$\tau_{avg} = (B_1\tau_1^2 + B_2\tau_2^2)/(B_1\tau_1 + B_2\tau_2) \quad (4)$$

In the equation, τ is the lifetime and B is the preexponential factor.

1. **Table S1** Crystal and refinement data for complexes **1** and **2**.

2. **Table S2** Selected bond lengths [Å] and angles [°] for complexes **1** and **2**.

3. **Fig. S1.** 1D dual-core $[Co(DCDPE^{2-})]_n$ chain in **1.**

4. **Fig. S2.** The infrared spectrums of **1** and **2**.

5. **Fig. S3.**TGA curves of **1** and **2**.

6. **Fig. S4.** Powder X-ray diffraction (PXRD) patterns of **1** and **2**.

7. **Fig. S5.** The change of the luminescent emission intensity of **1** (a) and **2** (b) in different pH solutions.

8. **Fig. S6.** Time-dependent emission spectra of **1** (a) and **2** (b) suspended in aqueous solutions.

9. **Fig. S7.** Time-dependent emission spectra of L ligands suspended in aqueous solutions.

10. **Fig. S8.** Comparison of the luminescent intensity of **1** (a) and **2** (b) in the presence of mixed organic solvents.

11. **Fig. S9.** Luminescent emission spectra of LEV and other quinolones in **1** at room temperature.

12. **Fig. S10.** Luminescent emission spectra of Ni^{2+} and other metal ions in **2** at room temperature.

13. **Fig. S11.** Time-resolved fluorescence spectra (symbols) with bi-exponential fit (solid lines) to the decay curves for **1** before and after addition of acac and LEV.

14. **Fig. S12.** Time-resolved fluorescence spectra (symbols) with bi-exponential fit (solid lines) to the decay curves for **2** before and after addition of acac and Ni^{2+}.

15. **Fig. S13.** PXRD patterns of **1** and **2** in various solutions

16. **Fig. S14.** Spectral overlap between the absorption spectra of acac and the excitation spectra of **1** and **2**.

17. **Fig. S15.** Spectral overlap between the absorption spectra of LEV and the excitation spectra of **1.**

18. **Fig. S16.** Spectral overlap between the absorption spectra of Ni^{2+} ions and the excitation spectra of **2**.

Table S1 Crystal data and structure refinements for **1** and **2**.

	1	**2**
Empirical formula	$C_{29}H_{22}CoN_3O_5$	$C_{76}H_{66}Co_2N_{14}O_{14}$
Formula weight	551.42	1517.28
Temperature/K	296(2)	296(2)
Crystal system	monoclinic	monoclinic
Space group	*C2/c*	$P2_1/n$
a/Å	14.1916(4)	12.6220(9)
b/Å	14.0430(5)	11.7644(9)
c/Å	26.3455(6)	23.5657(17)
α/°	90	90
β/°	92.889(2)	95.079(6)
γ/°	90	90
V/Å^3	5243.8(3)	3485.5(4)
Z	8	2
D_{calc} (g/cm^3)	1.397	1.446
μ/mm^{-1}	0.699	0.555
F(000)	2272.0	12.6220(9)
Crystal size/mm^3	0.21 × 0.19 × 0.18	0.21 × 0.21 × 0.19
Radiation	MoKα (λ = 0.71073)	MoKα (λ = 0.71073)
Θ range for data collection/°	4.314 to 61.024	4.742 to 61.158
Index ranges	-20 ≤ h ≤ 19, -18 ≤ k ≤ 19, -37 ≤ l ≤ 37	-16 ≤ h ≤ 17, -16 ≤ k ≤ 16, -33 ≤ l ≤ 29
Reflections collected	38274	56420
Independent reflections	7786 [R_{int} = 0.0369, R_{sigma} =0.0411]	8027 [R_{int} = 0.0549, R_{sigma} = 0.0413]
Data/restraints/parameters	7786/0/343	10181/48/503
Goodness-of-fit on F^2	1.030	1.021
Final R indexes [I>=2σ (I)]	R_1 = 0.0607, wR_2 = 0.1516	R_1 = 0.0505, wR_2 = 0.1107
Final R indexes [all data]	R_1 = 0.1103, wR_2 = 0.1774	R_1 = 0.0844, wR_2 = 0.1267
Largest diff. peak/hole / e Å^{-3}	0.52/-0.42	1.09/-0.72

Table S2 Selected bond lengths [Å] and angles [°] for the **1** and **2**.

Parameter	Value	Parameter	Value
1			
Co1–O1	2.05 (2)	Co1–O1A	2.07 (19)
Co1–O5B	2.17(2)	Co1–O4B	2.15(3)
Co1–N3	2.16(3)	Co1–N1	2.10(2)
N1–Co1–N3	75.85(10)	O1–Co1–O1B	77.49(7)
O1B–Co1–O5B	88.18(8)	O1–Co1–O5B	161.85(8)
O1B–Co1–O4B	98.49(8)	O1B–Co1–O4B	98.49(8)
O1–Co1–O4B	109.52(9)	O1–Co1–N3	98.86(9)
O1B–Co1–N3	100.36(9)	O1B–Co1–N3	100.36(9)
O1B–Co1–N1	167.07(10)	O1–Co1–N1	90.78(8)
O1B–Co1–C12B	94.73(9)	O1–Co1–C12B	138.64(10)
O5B–Co1–C12B	30.60(9)	O4B–Co1–O5B	61.22(8)
O4B–Co1–N3	148.69(9)	O4B–Co1–C12B	30.64(9)
N3–Co1–O5B	94.59(8)	N3–Co1–C12B	122.48(10)
N1–Co1–O5B	104.36(9)	N1–Co1–O4B	90.49(10)
N1–Co1–C12B	97.71(10)		
2			
Co1–O2	2.03(16)	Co1–O4	2.09 (15)
Co1–N3	2.12(17)	Co1–N4	2.16(18)
Co1–N6A	2.13(18)	Co1–N7A	2.18(18)
O2–Co1–O4	86.09(6)	O2–Co1–N6A	94.93(7)
O2–Co1–N7A	87.50(7)	O4–Co1–N3	90.78(6)
O4–Co1–N4	94.89(6)	O4–Co1–N6A	168.56(7)
O4–Co1–N7A	92.71(6)	N3–Co1–N4	76.18(7)
N3–Co1–N6A	89.26(7)	N3–Co1–N7A	98.35(7)
N4–Co1–N7A	170.67(7)	N6A–Co1–N4	96.22(7)
N61–Co1–N7A	75.97(7)		

Symmetry codes for **1**: A: 1/2–*x*, 3/2–*y*, 1–*z*; B: 1/2+*x*, 3/2–*y*, 1/2+*z*; C: 1–*x*, +*y*, 1/2–*z*; For **2**: A: 1–*x*, 1–*y*, 1–*z*; B: 3/2–*x*, 1/2+*y*, 3/2–*z*; C: 2–*x*, 2–*y*, 1–*z*;

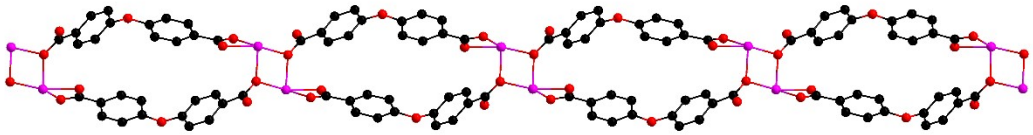

Fig. S1. 1D dual-core $[Co(DCDPE^{2-})]_n$ chain in **1**.

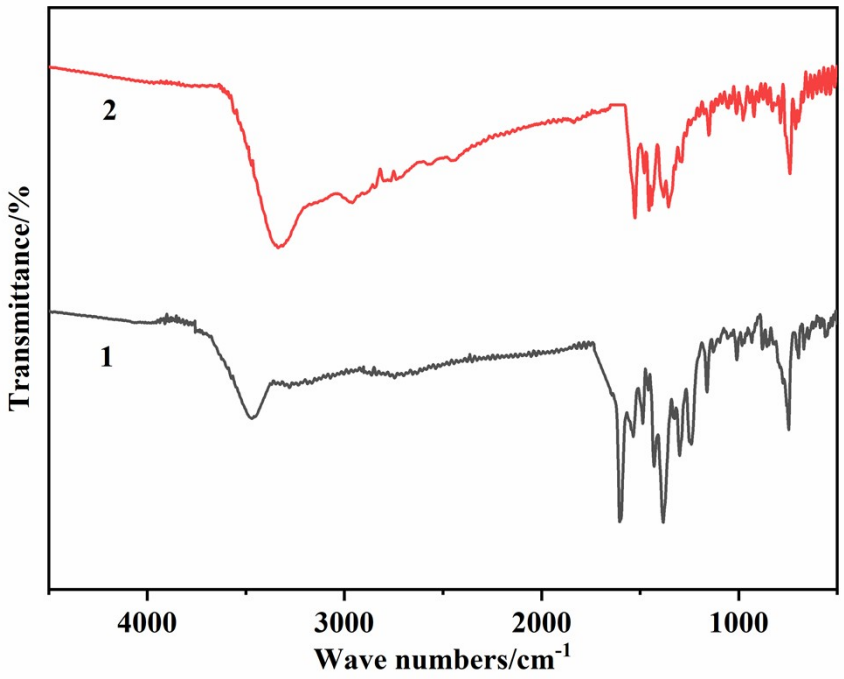

Fig. S2. The infrared spectrums of **1** and **2**.

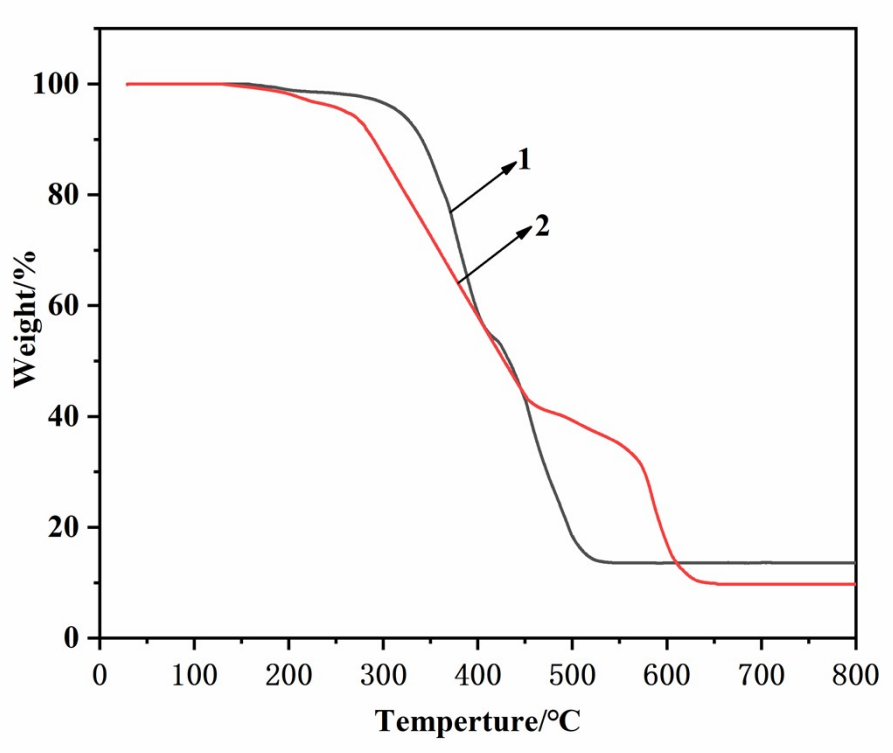

Fig. S3. TGA curves of **1** and **2**.

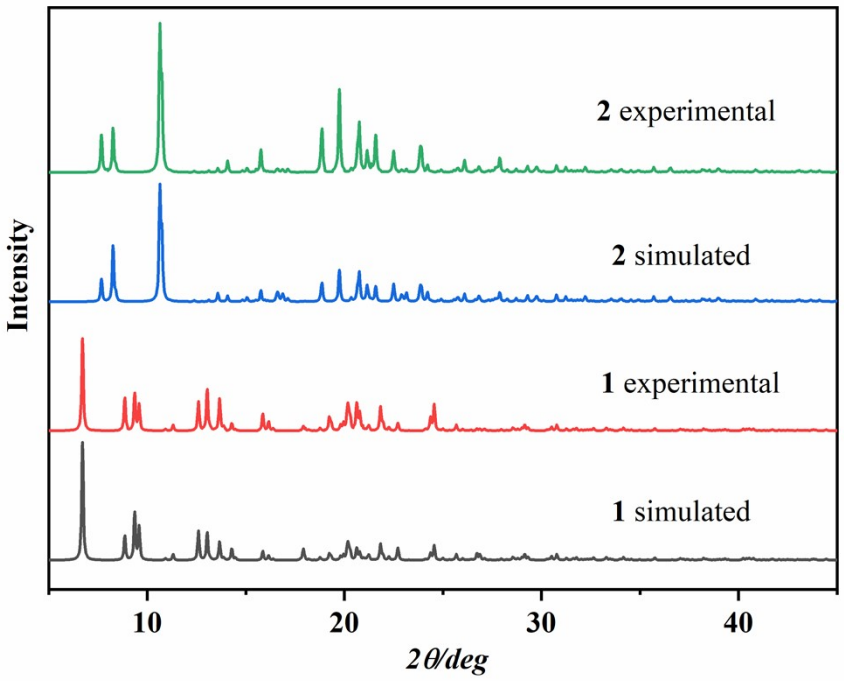

Fig. S4. Powder X-ray diffraction (PXRD) patterns of **1** and **2**.

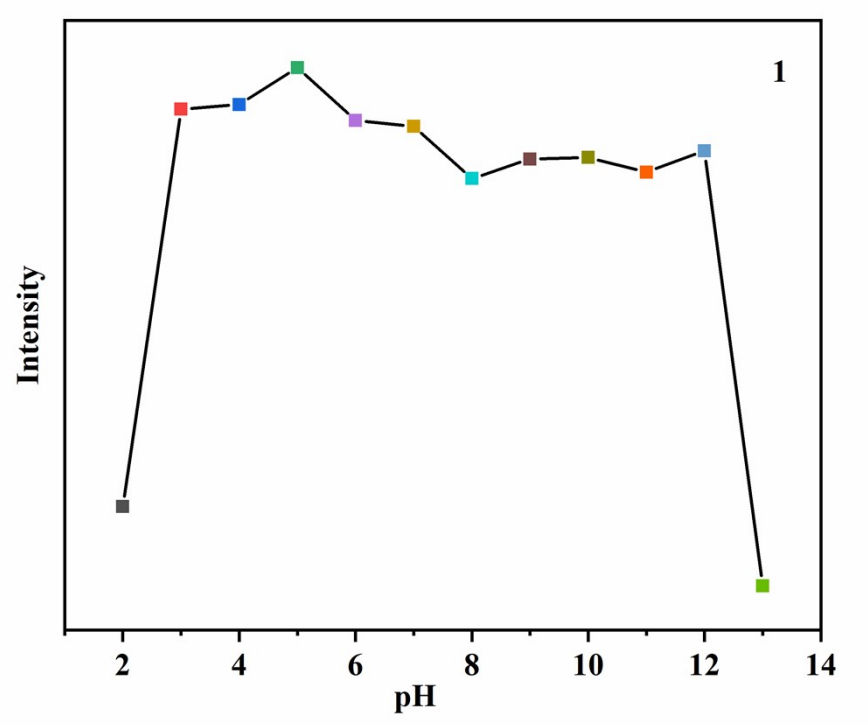

(a)

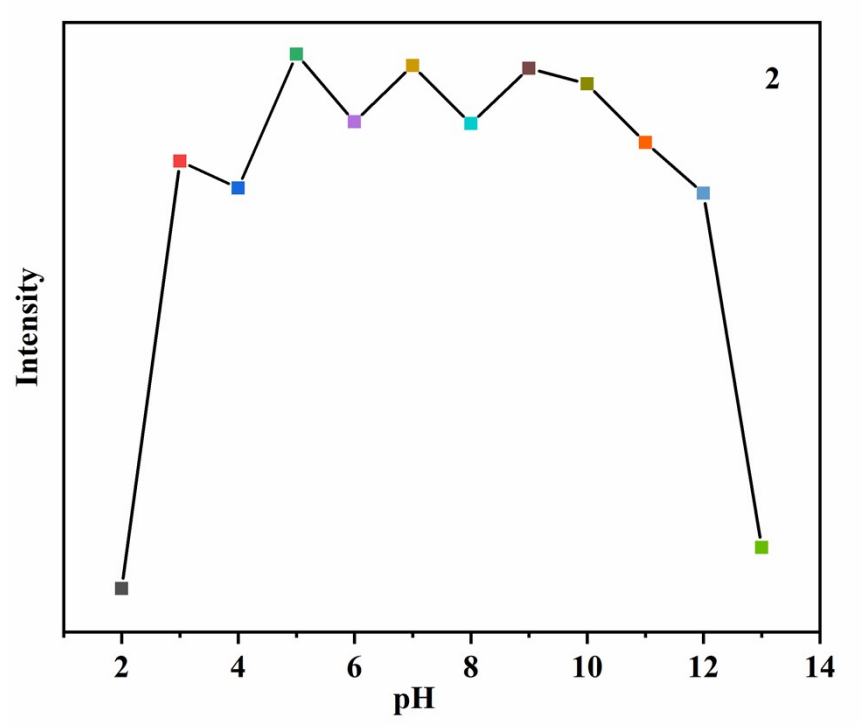

(b)

Fig. S5. The change of the luminescent emission intensity of **1** (a) and **2** (b) in different pH solutions.

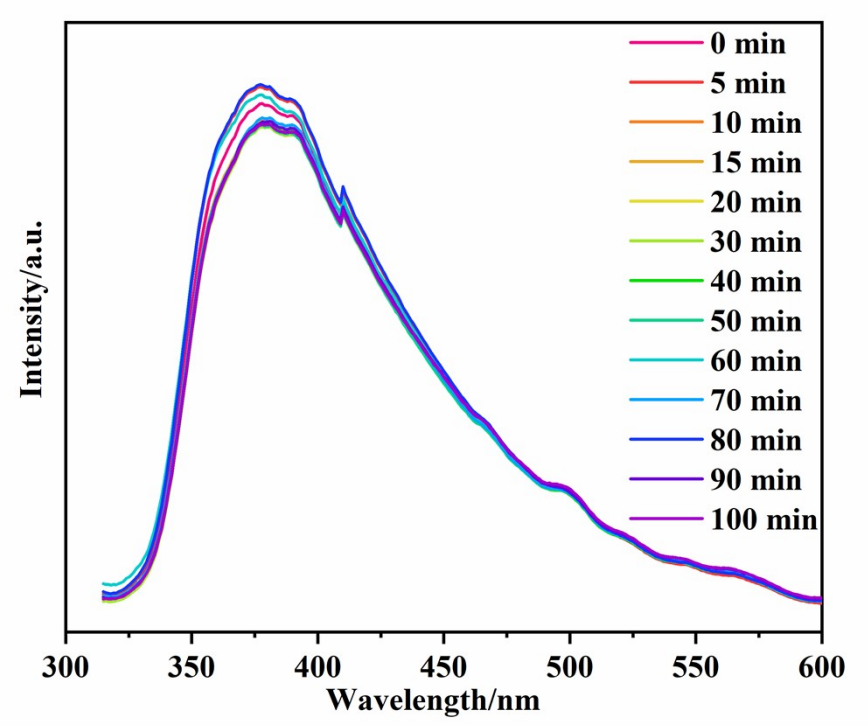

(a)

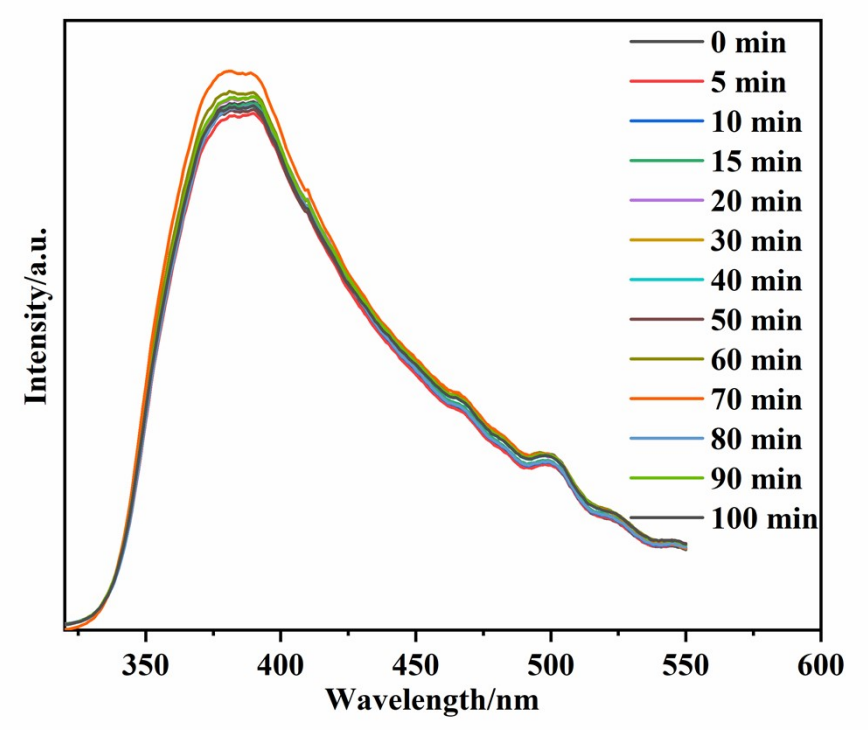

(b)

Fig. S6. Time-dependent emission spectra of **1** (a) and **2** (b) suspended in aqueous solutions.

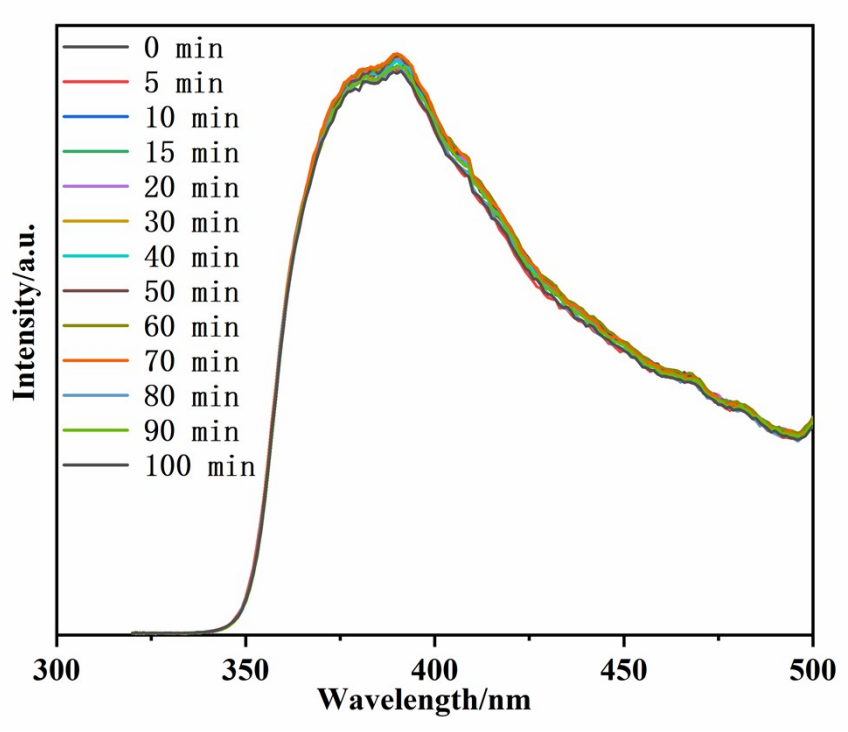

Fig. S7. Time-dependent emission spectra of L ligands suspended in aqueous solutions.

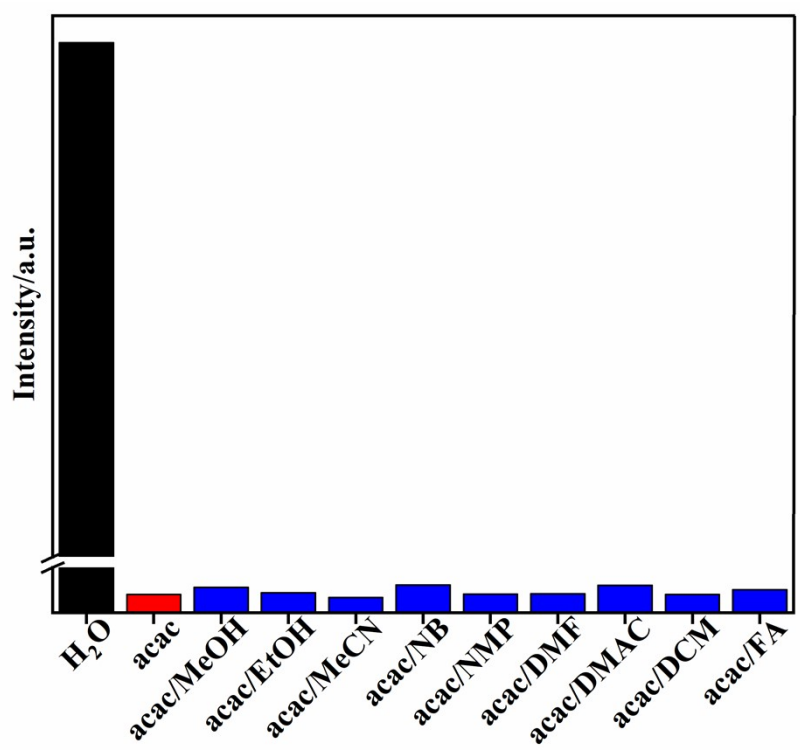

(a)

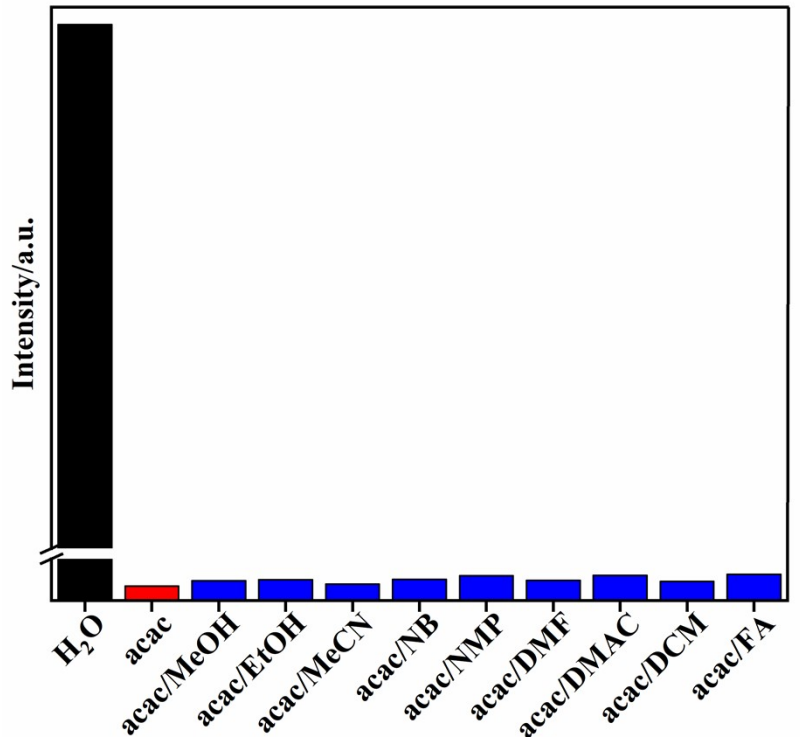

(b)

Fig. S8. Comparison of the luminescent intensity of **1** (a) and **2** (b) in the presence of mixed organic solvents.

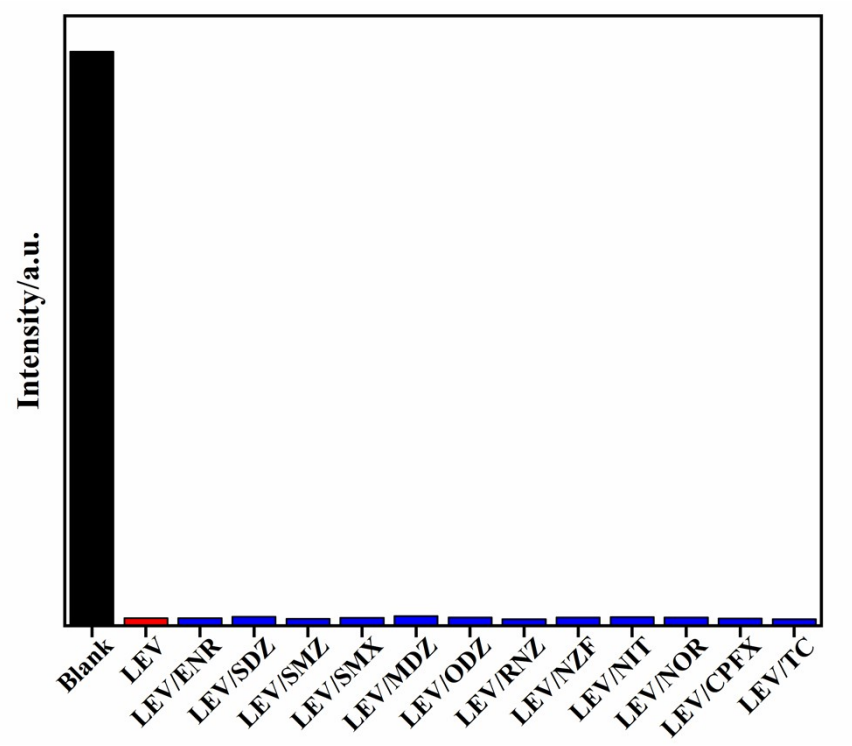

Fig. S9. Luminescent emission spectra of LEV and other quinolones in **1** at room temperature.

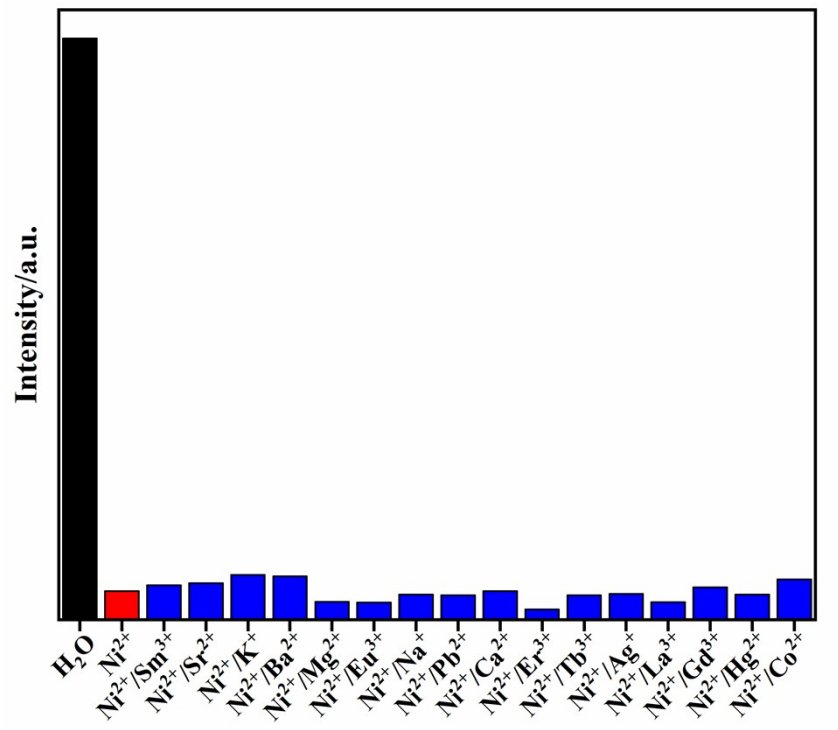

Fig. S10. Luminescent emission spectra of Ni^{2+} and other metal ions in **2** at room temperature.

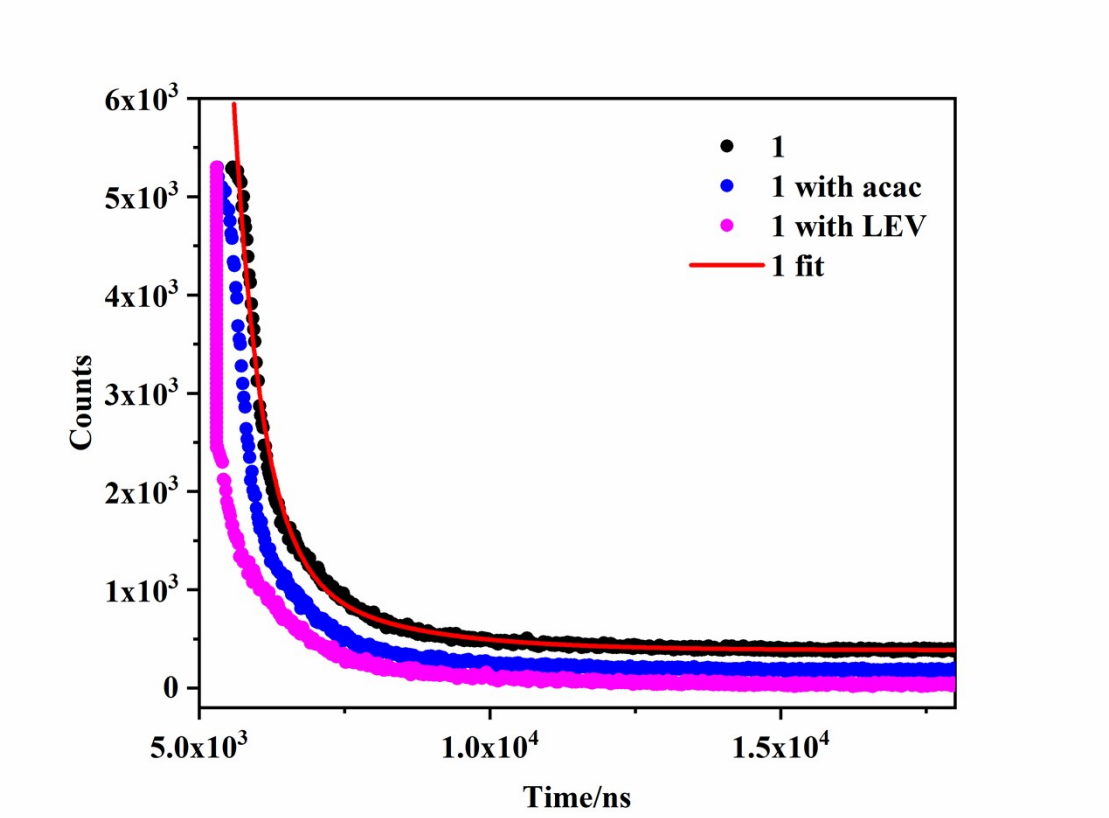

Fig. S11. Time-resolved fluorescence spectra (symbols) with bi-exponential fit (solid lines) to the decay curves for **1** before and after addition of acac and LEV.

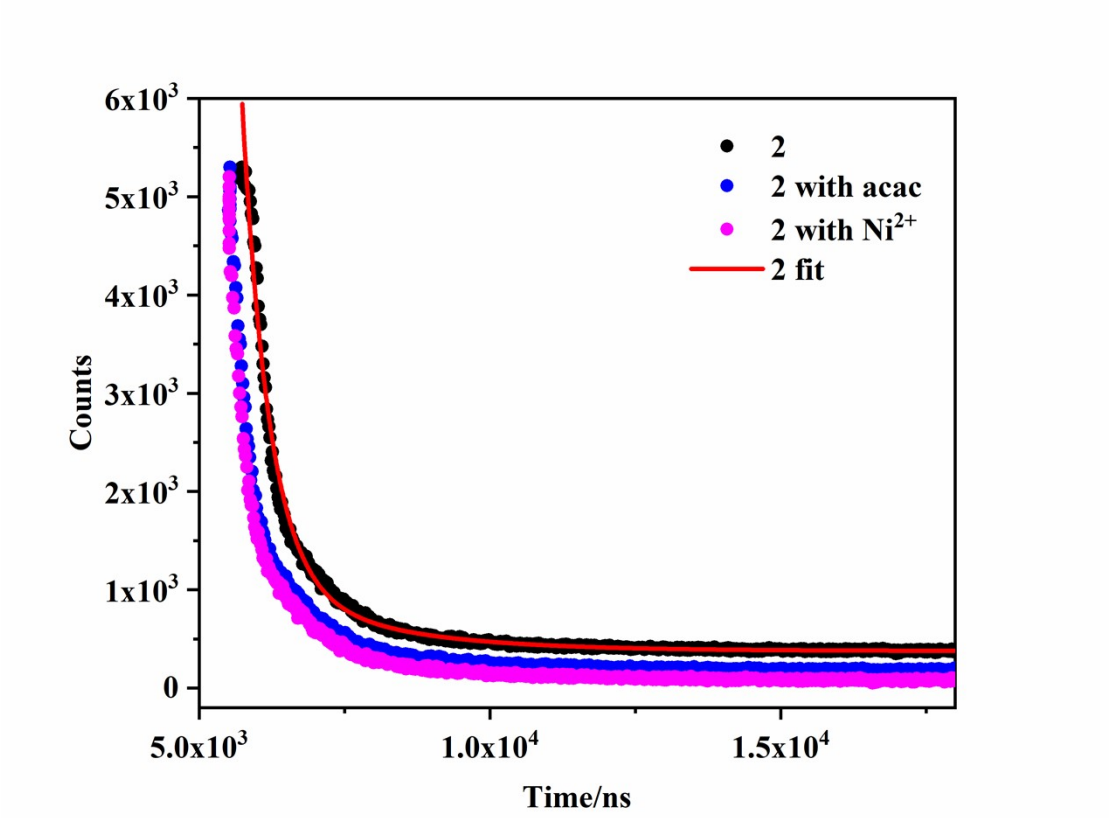

Fig. S12. Time-resolved fluorescence spectra (symbols) with bi-exponential fit (solid lines) to the decay curves for **2** before and after addition of acac and Ni^{2+}.

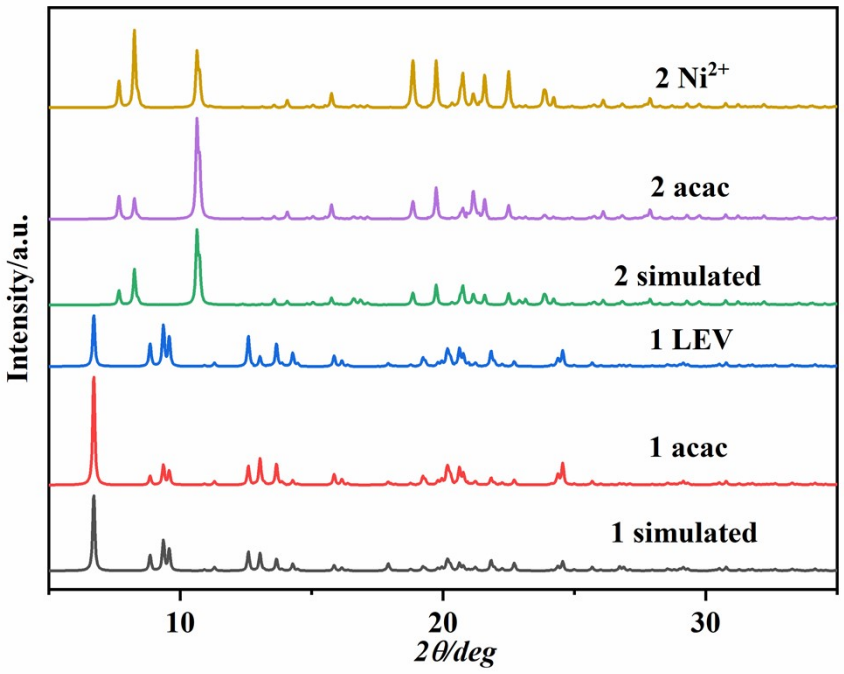

Fig. S13. PXRD patterns of **1**and **2** in various solutions

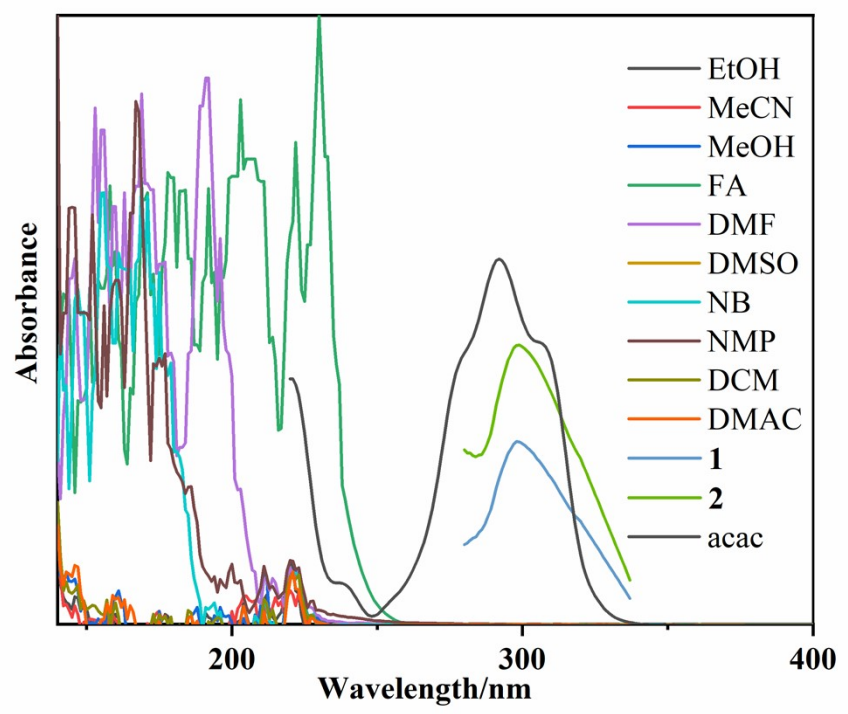

Fig. S14. Spectral overlap between the absorption spectra of acac and the excitation spectra of **1** and **2**.

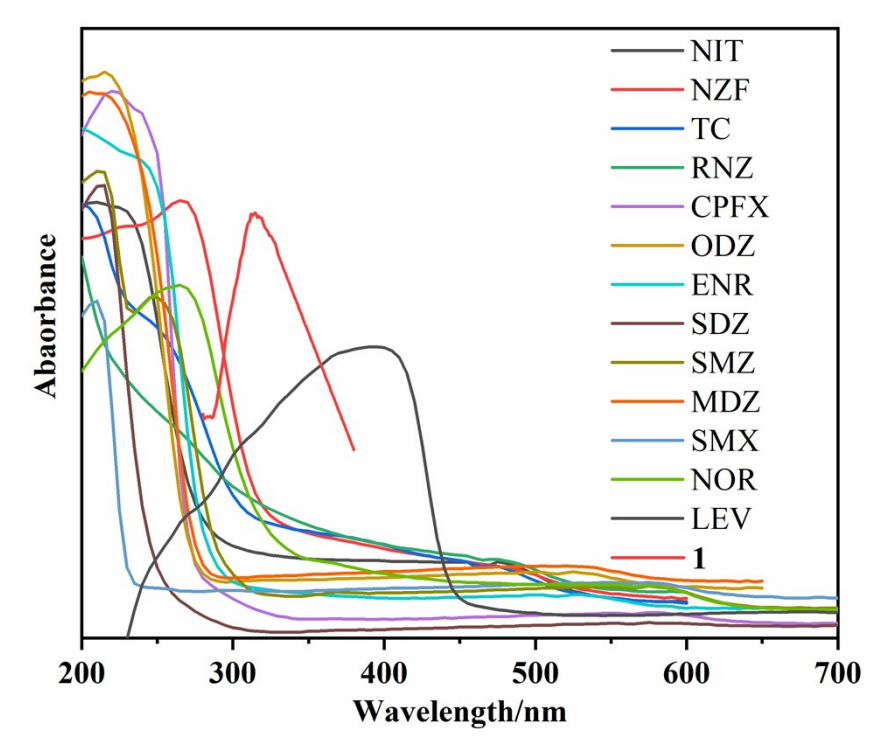

Fig. S15. Spectral overlap between the absorption spectra of LEV and the excitation spectra of **1.**

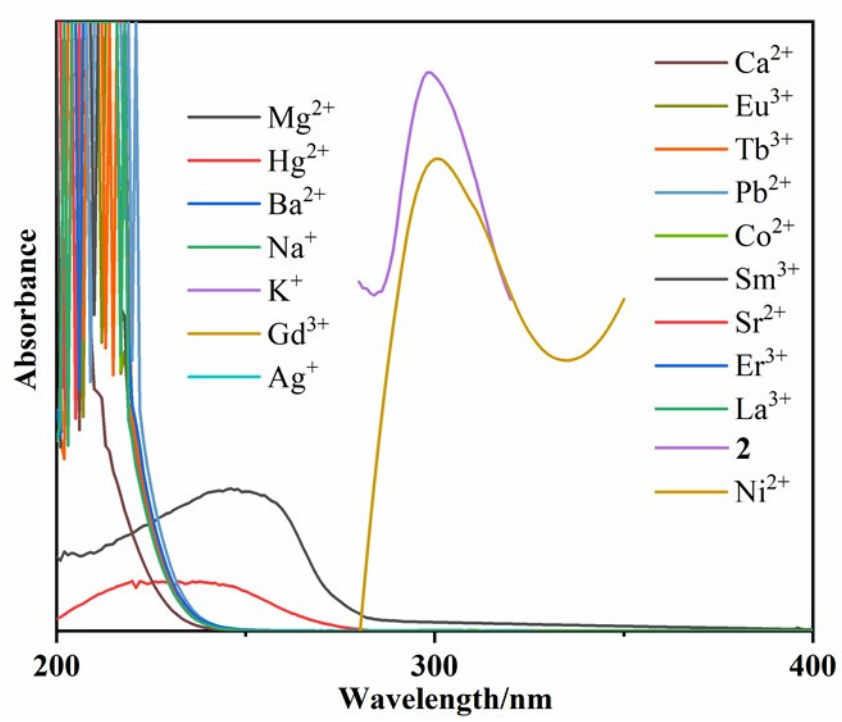

Fig. S16. Spectral overlap between the absorption spectra of Ni^{2+} ions and the excitation spectra of **2**.